J Mater Sci (2009) 44:257–265
DOI 10.1007/s10853-008-3052-9

Effectiveness of Ni-based diffusion barriers in preventing hard zone formation in ferritic steel joints

R. Anand · C. Sudha · T. Karthikeyan · A. L. E. Terrance · S. Saroja · M. Vijayalakshmi

Received: 3 October 2007 / Accepted: 15 October 2008 / Published online: 10 November 2008

Abstract A numerical procedure based on finite difference method was used to simulate the formation of 'hard' and 'soft' zones, in dissimilar weldments of 9Cr–1Mo and 2¼Cr–1Mo steels during high temperature exposure. Kinetic analysis of the calculated diffusion profiles showed that the activation energy for carbon diffusion in Cr–Mo steels is marginally higher than that in Fe–C system. Calculations were extended to incorporate the effect of Ni-based interlayers between 2¼Cr–1Mo and 9Cr–1Mo ferritic steels. The presence of a diffusion barrier was found to reduce the propensity for formation of hard and soft zones, which is related to the interaction parameter ε_C^M. Thickness of the interlayer required to suppress the formation of hard zone was optimized by the calculations. Transition joints of ferritic steels with Inconel 182 as the interlayer of thickness close to that predicted by the computations were fabricated and exposed to elevated temperature. Microstructural studies and hardness measurements further confirmed the effectiveness of Ni-based interlayers in preventing hard zone formation.

Introduction

Ferritic steels are important structural materials in the steam generator circuit of thermal and nuclear power plants. The weld joints between dissimilar ferritic steels of large components are the potential zones for failure during service exposure. When dissimilar weldments between ferritic steels are exposed to high temperature, significant microchemical and consequent microstructural changes are observed [1–4] at the interface, for example, the formation of hard and soft zones. At temperatures higher than 873 K a 'soft zone' is frequently observed at the 2¼Cr–1Mo side of 9Cr–2¼Cr weldment which is characterized by (a) low hardness of ~120 VHN and (b) the absence of carbides. A 'hard zone' is also observed on the 9Cr–1Mo side which is characterized by (a) high hardness (~282 VHN) and (b) high volume fraction of carbides. Since these zones are susceptible to failure under cyclic loading conditions, the study of such microstructural changes in dissimilar joints assumes industrial importance. The present paper deals with the formation of hard and soft zones in dissimilar weld joints between ferritic steels and demonstrates by computation and experiments a method to avoid their occurrence.

Computational studies on carburization [5–8] in Fe- and Ni-based systems have been the forerunner for similar studies in dissimilar joints. The approach adopted for the carburization of alloys has been extended to the study of formation of hard and soft zones at the interface of dissimilar weldments of ferritics, on exposure to high temperature. Buchmayr [9] has proposed a numerical model, along similar lines as that of Kirkaldy [10], to describe the simultaneous precipitation and dissolution of carbides across the fusion line of dissimilar weldments at high temperatures. The development of a carbon-depleted zone on low Cr side and a carbon-enriched zone on the high Cr side was simulated for weldments of 1Cr–Mo–V cast steel and 12Cr–Mo–V martensitic steel. Engström et al. [11] used a general model on multicomponent diffusion and multiphase precipitation to predict the carburization profiles of several Ni–Cr alloys and dissimilar weldments of Cr–Mo–V steels.

R. Anand · C. Sudha · T. Karthikeyan · A. L. E. Terrance · S. Saroja (✉) · M. Vijayalakshmi
Physical Metallurgy Division, Metallurgy and Materials Group, Indira Gandhi Centre for Atomic Research, Kalpakkam 603 102, India
e-mail: saroja@igcar.gov.in

The equilibrium calculations were made using Thermo-calc software, which was based on the concept of Gibbs energy minimization, and the model for diffusion was implemented using DICTRA. Kozeschink et al. [12, 13] determined various phase distribution and carbon diffusion profiles in 2Cr/0.5CrMoV and 2¼Cr/9Cr weldments after accounting for simultaneous diffusion and precipitation/dissolution of carbides using MATCALC and DICTRA packages.

Based on the understanding gained from the above studies on the mechanism of formation of the deleterious zones, many methods have been identified for their suppression. They include use of (1) interlayers acting as diffusion barriers for carbon, (2) graded chromium composition, or (3) base metal with altered composition to reduce the activity gradient. Influence of a 50 μm thick pure Ni layer between carbon steel and stainless steel has been studied by Kucera et al. [14]. They have shown that diffusion coefficient of elements on either side of the weld joint would influence the diffusion process leading to the formation of zones at higher temperatures (>1,073 K) after long exposure times. Evaluation of carbon profiles by computation in dissimilar weldments of ferritics with Ni-based interlayer has not been carried out so far. Experimental studies have been carried out [15] on transition joints of 2¼Cr–1Mo ferritic steel and AISI 304L austenitic steel with Ni-based (70 wt% Ni–15% Cr–9% Fe–0.10% C) or Fe-based (80 wt% Fe–24% Cr–0.10% C) filler materials. Decarburized and carburized zones were found to be present in the weldment with Fe-based filler material while carbon diffusion was suppressed with a reduced decarburized zone in a Ni-based filler material. This suggested the preference of Ni-based filler materials as diffusion barriers.

A direct microstructural evidence in support of the mechanism of formation of hard and soft zones has been provided by Kim et al. [1] in a dissimilar joint between ferritic steel and 309L austenitic stainless steel after PWHT. In our earlier work Sudha et al. [16–18] have studied in detail the dissimilar joints of 2¼Cr–1Mo/9Cr–1Mo ferritic steel and provided direct evidence for the formation of hard zone due to diffusion of carbon across the interface, which is also supported by similar studies in other systems [19, 20].

Based on the understanding of the atomistic processes in these studies, an attempt has been made to evolve a methodology to predict and prevent the formation of the deleterious zones. The present paper deals with the following aspects of formation of hard zone in the 2¼Cr/9Cr dissimilar joints:

- Computation of diffusion profiles to simulate hard and soft zone formation
- Kinetic analysis of the computed diffusion profiles
- Effect of Ni-based interlayers on the formation of hard zone
- Experimental confirmation of the predictions.

Computation and experimental details

Computational procedure

A ternary system of Fe–M–C type is being examined, where 'M' indicates major substitutional alloying element like Cr, Ni, or Mo. In the present case, the element considered is Cr, whose concentration is 2.25 wt% on one side and 10.25 wt% on the other side of the infinite diffusion system. At time $t = 0$, the composition on either side of the interface is the same as that of base and filler metals, i.e., the 'as welded' condition. On exposure to high temperature for finite time t_0, mass transfer is expected to take place following Fick's laws of diffusion, and the consequent concentration profiles for various elements across the interface are calculated using finite difference technique. The system of two different ferritic steels is assumed to be divided into large number of slabs parallel to the interface plane, with the appropriate boundary conditions: (1) at distances far away from the interface, the composition is the same as that of the original system and (2) at the interface between systems, the flux of the diffusing element is assumed to be continuous. Detailed flow chart of the computational procedure is given in Fig. 1 and details of the calculation are given in Appendix.

Experimental details

The bead on plate weldments were fabricated between 2¼Cr–1Mo and 9Cr–1Mo ferritic steels with Inconel 182 (containing 66 wt% Ni) as the interlayer. Figure 2 shows the schematic of the transition joint fabricated. The composition of 2¼Cr–1Mo base plate, Inconel 182, and 9Cr–1Mo electrodes are given in Table 1 and the welding parameters are given in Table 2. The thickness of Inconel 182 interlayer introduced between the ferritic steels was 0.1 mm.

These transition joints were subjected to post-weld heat treatment (PWHT) at 1,023 K for times from 1 to 15 h. After PWHT, the weldments were polished and etched using Vilella's reagent for microstructural examination. Vilella's reagent etches only the ferritic steels facilitating easier observation of the Ni-based interlayer. Microstructural examination was carried out using an Optical Microscope (Model No: MEF4A of M/s Leica) and microhardness measurements were made using Vickers

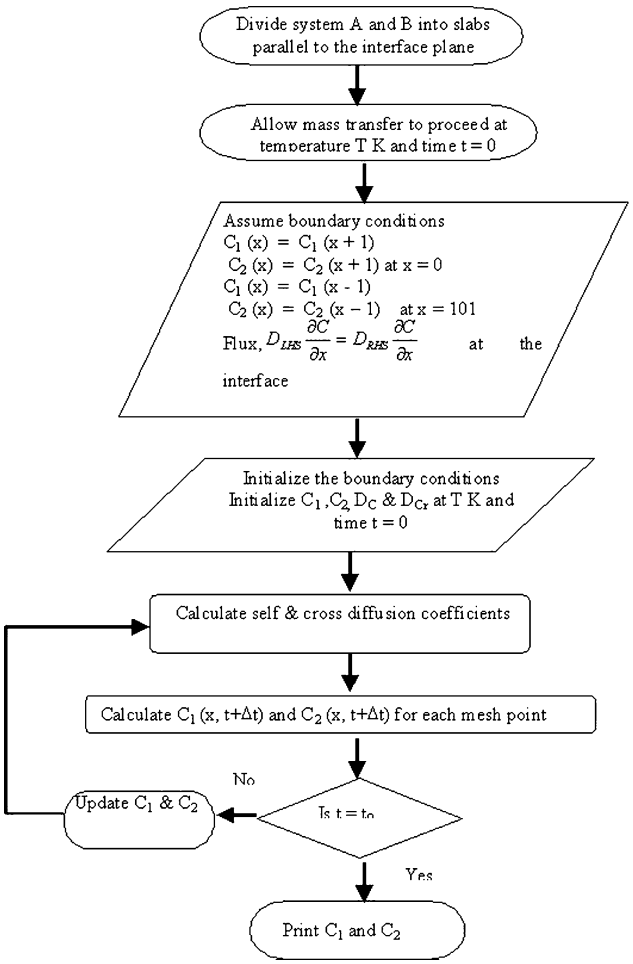

Fig. 1 Flow chart of the computational procedure

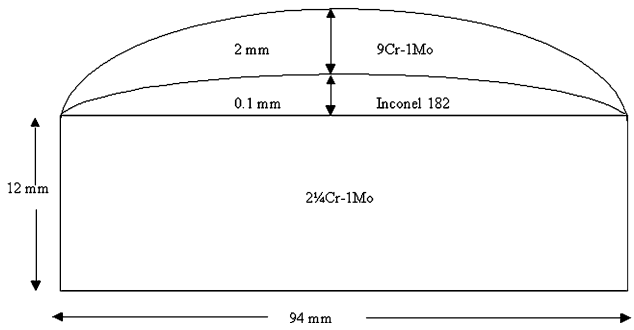

Fig. 2 Schematic of the transition weld under study

microhardness tester (M/s Leitz) with an applied load of 100 g.

Results

Results of the present study are discussed in the following sequence: (a) Computation of carbon diffusion profiles, (b) Kinetic analysis of the computed diffusion profiles, (c) Influence of Ni-based interlayer on the formation of hard zone and optimization of its thickness, and (d) Experimental confirmation of the computational predictions.

Computation of carbon diffusion profiles

Carbon diffusion profiles were computed using the method given in Appendix for various temperatures in the range of 823–1,023 K for different times. Figure 3a shows the carbon concentration profiles computed for a PWHT temperature of 1,023 K for the time duration of 1–15 h. Since the carbon content on both sides of the interface is the same ($\sim$0.1 wt%), no change is expected in the carbon concentration profiles. However, there is a deviation from conventional diffusion profiles, with a decrease in carbon content near the interface on 2¼Cr side forming a carbon-depleted zone of about 50 μm thickness (at 15 h), called as 'soft zone.' On the 9Cr side, a carbon-enriched zone of thickness of about 20 μm formed near the weld interface, which was called the 'hard zone.' Figure 3b shows the experimental evidence for the presence of hard and soft zones in a dissimilar weldment between 9Cr–1Mo/2¼Cr–1Mo ferritic steels subjected to PWHT at 1,023 K for 15 h [16]. The hard zone is manifested as a dark etched region (marked as 'A' in Fig. 3b) and soft zone as a light etched region (marked as 'B' in Fig. 3b). Hardness profile for the same temperature and time is superimposed on the optical micrograph, which shows a high hardness of around 282 VHN in region 'A' and a low hardness of around 120 VHN in region 'B.'

Kinetic analysis of the computed diffusion profiles

Carbon concentration profiles were simulated for various PWHT temperatures—823, 873, 923, 973, and 1,023 K for

Table 1 Chemical composition of the base plate and electrodes

S. No.	Description	Element (wt%)										
		C	Cr	Mo	Mn	S	P	Si	Ni	Nb	Ti	Fe
1.	2¼Cr–1Mo Plate	0.12	2.18	1.0	0.46	0.001	0.01	0.25	–	–	–	Balance
2.	9Cr–1Mo weld metal (Electrode)	0.08	10.25	0.98	0.91	0.02	0.02	0.40	–	–	–	Balance
3.	Inconel 182 (Electrode)	0.05	13.8	–	7.84	0.004	0.01	0.56	66	1.84	0.4	Balance

Table 2 Welding parameters employed for preparation of the bead on plate welds

S. No.	Base material	Electrode	Electrode Diameter (mm)	Current (A)	Voltage (V)	Speed (mm/min)
1.	2¼Cr–1Mo	Inconel 182	3	80	22	140
2.	Inconel 182	9Cr–1Mo	5	80	22	140

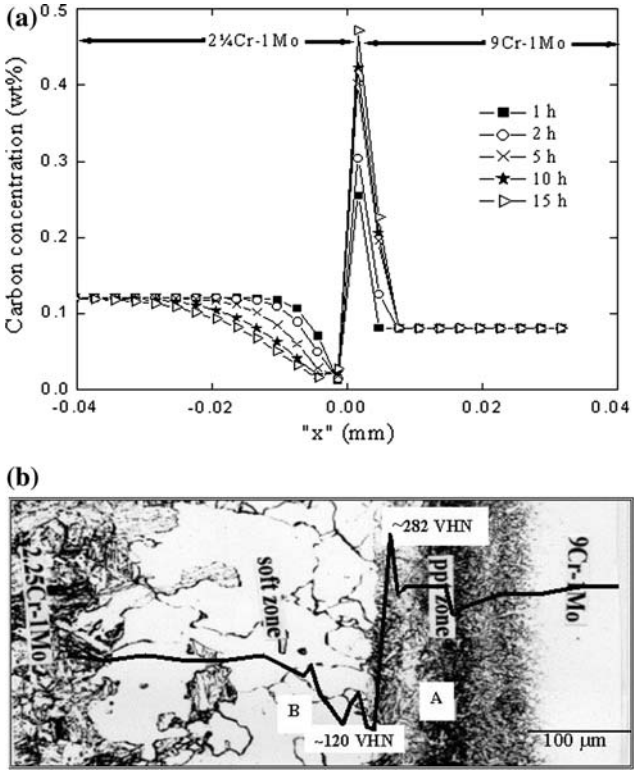

Fig. 3 **a** Simulated carbon concentration profiles for PWHT at 1,023 K for durations ranging from 1 to 15 h, where '*x*' is the distance from the interface in mm. **b** Experimental evidence for the formation of hard zone (marked as 'A') and soft zone (marked as 'B') in dissimilar weldment of 2¼Cr–1Mo and 9Cr–1Mo ferritic steels [16] after PWHT at 1,023 K for 15 h. Hardness profile for the same temperature and time is superimposed showing a high hardness (~282 VHN) in region 'A' and a low hardness (~120 VHN) in region 'B'

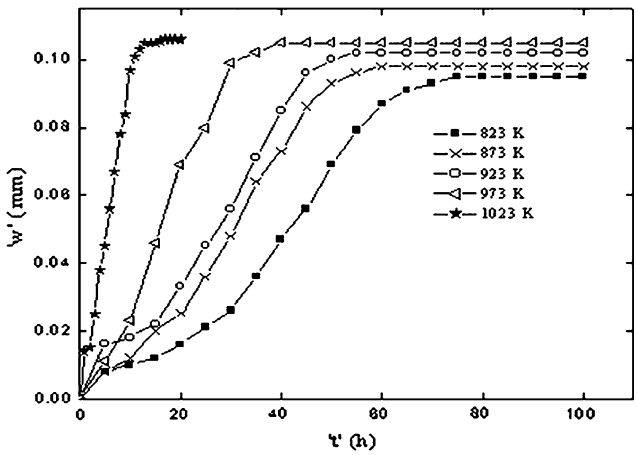

Fig. 4 Variation of zone width (*w* in mm) as a function of time (*t* in hour) for PWHT at 823, 873, 923, 973, and 1,023 K

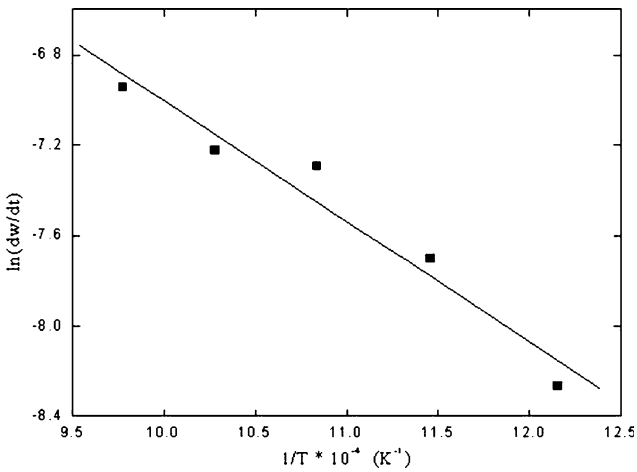

Fig. 5 Arrhenius plot using zone width (*w* in mm) obtained by computational methods as the kinetic parameter

durations up to 500 h using the method explained in the previous section. The growth kinetics of the zones was studied using these concentration profiles. The diffusion zone width '*w*,' which is taken as the sum of the widths of carbon-depleted and carbon-enriched regions in the concentration vs. distance profile, was measured as a function of temperature and time and is shown in Fig. 4. The temperature dependence of the variation of width with time in Fig. 4 shows the following features: (i) significant increase in the slope of linear part $\frac{dw}{dt}$ and (ii) decrease in time for saturation with increase in temperature. These are conventional signatures of a diffusion process following Arrhenius behavior. Since the slope of the curve changes continuously with respect to time, a fifth degree polynomial fit is made and differentiated to determine the slope $\frac{dw}{dt}$. Figure 5 shows the linear variation of $\ln\frac{dw}{dt}$ vs. $1/T$ for the calculated diffusion profiles. The activation energy for the diffusion process was calculated using the zone width (w) as the kinetic parameter. From the plot of $\ln\frac{dw}{dt}$ vs. $1/T$ (Fig. 5) the value of apparent activation energy was obtained as 0.92 eV. This compares with the activation energy for carbon diffusion in α-Fe matrix (0.83 eV) [21]. The higher value of activation energy obtained by the kinetic analysis is attributed to the presence of Cr in Fe, with an attractive influence on carbon ($\varepsilon_C^{Cr} = -72$ [22]). Having established the formation of hard and soft zones

across the interface in the weld joint during PWHT, it is necessary to adopt measures to prevent their formation to minimize degradation of the joint. One such method is described below.

Influence of Ni-based interlayer in preventing formation of hard zone and optimization of its thickness

Since it is established [16–18] that formation of hard and soft zones in a 2¼Cr–1Mo and 9Cr–1Mo dissimilar weldment is due to diffusion of carbon, driven by the activity gradient, it is reasonable to expect that an intermediate layer, which would decrease activity gradient and retard diffusion, will delay or decelerate the formation of hard zone. A Ni-based intermediate layer (Inconel 182) was selected since it repels carbon due to its high positive interaction parameter with carbon, i.e., $\xi_C^{Ni} = +2$ [23]. Activity is related to ε_C^M by the following equation:

$$a_C = C_1\left(\exp\left(C_1\varepsilon_C^C + C_M\varepsilon_C^M\right)\right) \quad (1)$$

where a_C is the activity of carbon, C_1 and C_M are the concentrations of carbon and element 'M' in solution, respectively, and ε_C^C and ε_C^M are the Wagner interaction parameters.

The carbon concentration profiles were evaluated (for PWHT temperature of 1,023 K for a duration of 15 h) for various thicknesses of Ni-based interlayer starting from 3 μm to 2 mm with a step size of 3 μm. Appropriate values were chosen for carbon content in solution in Ni, diffusion coefficient of carbon in Ni, and the interaction parameter between Ni and C in Inconel 182 for simulating the diffusion profiles.

Figure 6a–c shows the diffusion profiles of carbon for three different thicknesses of Inconel 182 interlayer—40, 80, and 100 μm, respectively. A significant reduction in the maximum carbon concentration is observed at the 9Cr/Ni interface (Fig. 6b, c). The presence of hard zone in a 40 μm thick interlayer, while its absence for higher thickness, is clearly revealed. Maximum carbon content in the hard zone decreases with increase in thickness of Inconel 182 interlayer and becomes equal to the carbon concentration in solution on the 9Cr–1Mo weld metal (Fig. 6b) beyond a thickness of 80 μm. Hence, based on the computation it can be predicted that a Ni-based interlayer of thickness 80 μm is sufficient to suppress the formation of hard zone.

Experimental confirmation of the computational predictions

In order to verify the prediction on the formation of hard and soft zones, transition joints were fabricated in the form of bead on plate welds between 2¼Cr–1Mo and 9Cr–1Mo ferritic steels with 0.1 mm thick Inconel 182 as the interlayer (Fig. 2). Inconel 182 is preferred as an interlayer between ferritic steels due to the following reasons: (1) it exhibits intermediate thermal expansion coefficient between 2¼Cr–1Mo and 9Cr–1Mo and (2) it has better mechanical properties and easy weldability. Preliminary studies were carried out with weld joints fabricated with Ni-based interlayer.

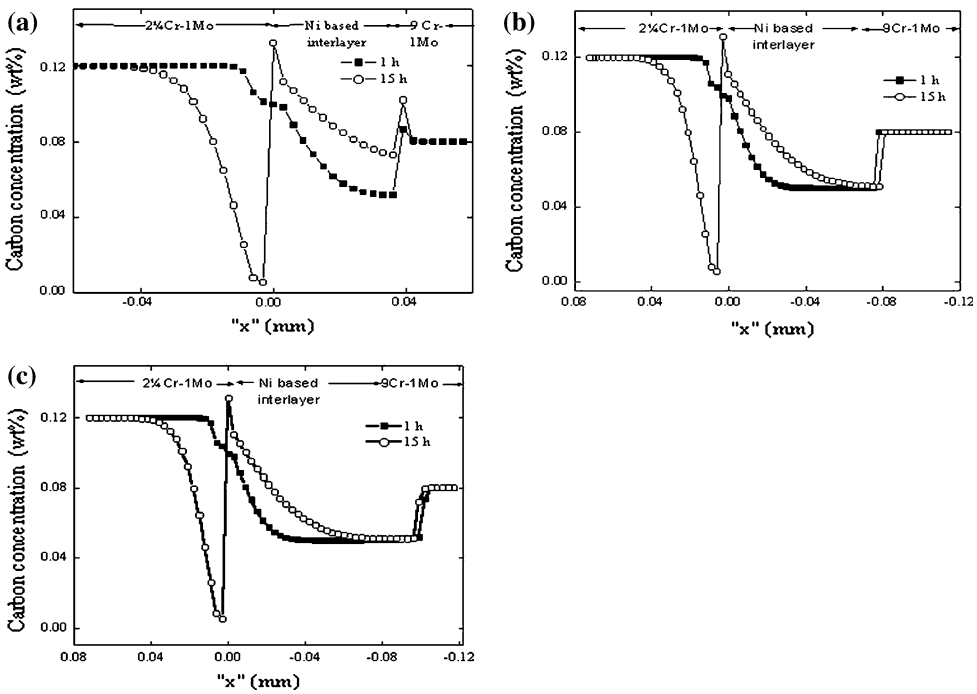

Fig. 6 Diffusion profiles of carbon after PWHT at 1,023 K for 15 h with Ni-based interlayer (Inconel 182) of different thickness **a** 40 μm, **b** 80 μm, and **c** 100 μm. Note the carbon content is equal to the 9Cr–1Mo carbon content in **b** and **c** in contrast to high carbon content in **a**

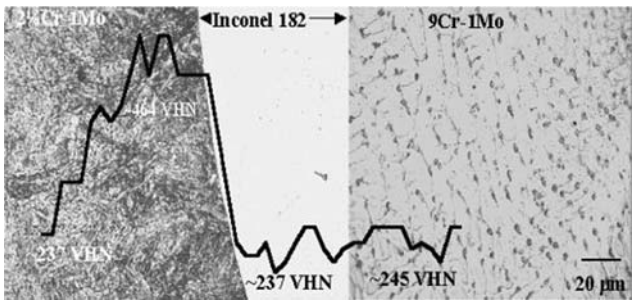

Fig. 7 Optical microstructure and hardness profile of 'as welded' transition joint with an interlayer of thickness 0.1 mm

Figure 7 shows the optical microstructure and superimposed hardness profile of the 'as welded' transition joint. The 2¼Cr–1Mo side showed predominantly a bainitic structure, while the 9Cr–1Mo side exhibited a solidification structure. Inconel 182 interlayer was not etched by the reagent. The interfaces between 2¼Cr–1Mo/Inconel 182 and 9Cr–1Mo/Inconel 182 were quite sharp and distinct. Superimposed microhardness profile (Fig. 7) showed an average hardness of 237 VHN on 2¼Cr–1Mo, Inconel 182 interlayer, and 9Cr–1Mo. Hardness of about 450 VHN was observed in the heat-affected zone of 2¼Cr–1Mo base metal.

The microstructure and hardness profile of the transition joints after PWHT at 1,023 K for 1 and 15 h are shown in Fig. 8a and b, respectively. A bainitic structure is observed close to the interface in 2¼Cr–1Mo, while the 9Cr–1Mo side showed a solidification structure. Careful examination of the interface between Inconel 182 and 9Cr shows the absence of hard zone, in sharp contrast to that of a dissimilar weldment without the interlayer (Fig. 3b). The observation that Ni interlayer decreases the propensity for formation of hard zone and that optimum thickness of the interlayer is 100 μm supports the predictions based on computation. However, for a weldment heat-treated beyond 10 h a thin dark etched region was observed at the interface of 2¼Cr–1Mo and Inconel 182 (marked as 'C' in Fig. 8b). The width or thickness of this region did not show any systematic variation with the heat treatment conditions. The reason for the formation of this region is being analyzed.

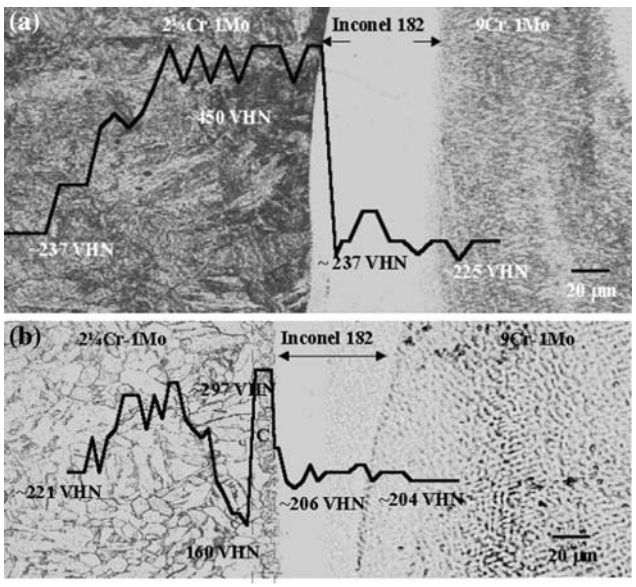

Fig. 8 Optical microstructure and hardness profile showing the absence of hard and soft zones in a transition joint having 0.1 mm thick Inconel 182 interlayer subjected to PWHT at 1,023 K for **a** 1 and **b** 15 h

Discussion

The computation of carbon profiles (Fig. 3a) using finite difference method as described in Appendix simulated the formation of hard and soft zones in a ferritic dissimilar joint. Despite the fact that carbon content on both sides of the interface (2¼Cr–1Mo and 9Cr–1Mo) were comparable, significant redistribution of carbon was observed at the interface leading to carbon-rich hard zone and carbon-depleted soft zone at the high and low chromium sides, respectively. This has been understood in terms of activity gradient across the weldment from low Cr (high activity $a_C = 0.063$ [2]) to high Cr (low activity 0.0033 [2]) side, in response to which diffusion of carbon occurs at elevated temperature. Consequently, carbides on the low Cr side dissolve, eventually forming the 'soft zone' near the interface. Dissolution of carbides removes the pinning centers permitting free migration of ferrite boundaries and excessive grain growth. The carbon, which diffuses to the high Cr side, gets precipitated forming the 'hard zone' near the interface. The maximum carbon content in the hard zone for 15 h is calculated to be 0.47 wt%, which agrees with the experimental results reported earlier [18].

The effect of a Ni-based diffusion barrier on carbon redistribution across two dissimilar ferritic steels has been studied. Our results show that the propensity for formation of hard zone is less in 2¼Cr/Ni/9Cr weldments. This can be understood in terms of the positive interaction parameter of nickel with carbon. The maximum amount of carbon in the hard zone or width of the hard zone can be used to evaluate the optimum thickness of the interlayer. The maximum amount of carbon in the hard zone was found to decrease with increase in the thickness of the interlayer.

Preliminary experimental studies carried out with 0.1 mm thickness of Inconel 182 interlayer revealed restructuring at the interfaces without any concomitant

increase in hardness. Although the formation of a bainitic structure in the 2¼Cr–1Mo steel is as expected, the 9Cr–1Mo weld metal shows a solidification structure (Fig. 7) with a hardness value of ~245 VHN. This is in contrast to the martensitic structure of high hardness of about 400 VHN, which is expected to form during quenching or normalizing. It is possible that diffusion of Ni from Inconel to 9Cr side would have suppressed the M_s (martensitic start) temperature preventing the formation of martensite during cooling. The high hardness (450 VHN) observed in the heat-affected zone of 2¼Cr–1Mo may be because during welding the base metal close to the weld metal is heated beyond the austenizing temperature. The consequent phase transformation of the high temperature austenite during cooling leads to high hardness on 2¼Cr–1Mo side. Such a high value of hardness in the heat-affected zone on 2¼Cr–1Mo side has also been reported in our earlier studies [16] on dissimilar weldments of 2¼Cr–1Mo and 9Cr–1Mo steel. The investigations based on microstructure and hardness measurements confirmed the absence of hard and soft zones supporting the predictions based on computation.

Observation of a dark etched region ['C' in Fig. 8b] at the interface of 2¼Cr–1Mo and Inconel 182 has been already reported in literature [15]. This region is not considered as the hard zone for the following reasons:

1. Absence of simultaneous enrichment of Cr and C in region 'C' which is otherwise expected in a hard zone.
2. Absence of change in the width and hardness of the zones with PWHT temperature and time unlike the hard and soft zones, which show systematic change.
3. Formation of region 'C' on the low Cr side of the weld interface.
4. Low width of region 'C' as compared to that of hard zone that formed in dissimilar weldments of 9Cr–1Mo/2¼Cr–1Mo ferritic steels for the same PWHT condition.

Conclusion

- A numerical method based on finite difference technique was used to solve ternary diffusion equations and simulate carbon diffusion profiles across the weld interface for various PWHT conditions in a dissimilar weldment of 2¼Cr–1Mo and 9Cr–1Mo ferritic steels.
- A nickel-based interlayer between 2¼Cr–1Mo and 9Cr–1Mo ferritic steels was found effective in suppressing the formation of hard zone. It was found that the propensity for formation of hard zone decreases with increase in thickness of the interlayer.
- Experimental investigations on 2¼Cr–1Mo/Inconel 182/9Cr–1Mo joints after PWHT agree well with computational predictions.

This study has demonstrated that the computational method based on finite difference technique can be used to predict the behavior of dissimilar weldments during exposure to high temperature with few preliminary experiments to confirm the predictions.

Acknowledgements The authors thank Dr. Baldev Raj, Director, IGCAR, and Dr. P. R. Vasudeva Rao, Director, Metallurgy and Materials Group, for their support and encouragement for this project. The authors also thank Dr. S. K. Albert and Dr. K. Laha, Scientific Officers, MMG, IGCAR, for their help and useful suggestions.

Appendix

Simulation of carbon diffusion profiles.

The sole objective of the model is to demonstrate the effectiveness of Ni-based interlayer in preventing the hard zone formation. For this purpose a simple single-phase model is considered, which does not take into account the precipitation of carbides.

The change in concentration of a diffusing element with respect to time can be obtained from the well-known Fick's second law of diffusion,

$$\frac{\partial C}{\partial t} = \frac{\partial}{\partial x}\left(D\frac{\partial C}{\partial x}\right) \tag{2}$$

where 'D' is the diffusion coefficient of the element in solid solution, 'C' is the concentration of the element in solution, 't' is the time, and 'x' is the distance. The system under consideration is a ternary system of Fe–M–C type where 'M' indicates any major substitutional alloying element like Cr, Ni, or Mo. In the present case, the major alloying element considered is Cr. For ternary diffusion, Fick's second law can be rewritten using Onsager's equation [5] as

$$\frac{\partial C_1}{\partial t} = \frac{\partial}{\partial x}D_{11}\frac{\partial C_1}{\partial x} + \frac{\partial}{\partial x}D_{12}\frac{\partial C_2}{\partial x} \tag{3}$$

$$\frac{\partial C_2}{\partial t} = \frac{\partial}{\partial x}D_{21}\frac{\partial C_1}{\partial x} + \frac{\partial}{\partial x}D_{22}\frac{\partial C_2}{\partial x} \tag{4}$$

where C_1 and C_2 refer to carbon and chromium concentration in solution. D_{11} and D_{22} are the self-diffusion coefficients of carbon and chromium in solution, respectively. D_{12} and D_{21} are the cross diffusion coefficients, which take into consideration the effect of one element on the other. Expanding the R.H.S. of Eqs. 3 and 4 we get

$$\frac{\partial C_1}{\partial t} = \frac{\partial D_{11}}{\partial x}\frac{\partial C_1}{\partial x} + D_{11}\frac{\partial^2 C_1}{\partial x^2} + \frac{\partial D_{12}}{\partial x}\frac{\partial C_2}{\partial x} + D_{12}\frac{\partial^2 C_2}{\partial x^2} \quad (5)$$

$$\frac{\partial C_2}{\partial t} = \frac{\partial D_{21}}{\partial x}\frac{\partial C_1}{\partial x} + D_{21}\frac{\partial^2 C_1}{\partial x^2} + \frac{\partial D_{22}}{\partial x}\frac{\partial C_2}{\partial x} + D_{22}\frac{\partial^2 C_2}{\partial x^2} \quad (6)$$

Since the contribution due to $\frac{\partial D_{11}}{\partial x}$, $\frac{\partial D_{12}}{\partial x}$, $\frac{\partial D_{22}}{\partial x}$, and $\frac{\partial D_{21}}{\partial x}$ is zero, they are neglected. Then the above equations can be simplified as

$$\frac{\partial C_1}{\partial t} = D_{11}\frac{\partial^2 C_1}{\partial x^2} + D_{12}\frac{\partial^2 C_2}{\partial x^2} \quad (7)$$

$$\frac{\partial C_2}{\partial t} = D_{21}\frac{\partial^2 C_1}{\partial x^2} + D_{22}\frac{\partial^2 C_2}{\partial x^2} \quad (8)$$

Using Schmit method [24] the differential Eqs. 7 and 8 can be transformed to finite differential equations using a one-dimensional grid of mesh points in space x and time t. The mesh points are separated by a space increment of Δx and time increment Δt. For carbon, the second differential of concentration with respect to space can be written as

$$\frac{\partial^2 C_1}{\partial x^2} = \frac{C_1[(x+1,t)] - 2C_1[x,t] + C_1[(x-1,t)]}{\Delta x^2} \quad (9)$$

and the first differential of concentration with respect to time is

$$\frac{\partial C_1}{\partial t} = \frac{C_1[x,(t+\Delta t)] - C_1[x,t]}{\Delta t} \quad (10)$$

Similarly for chromium,

$$\frac{\partial^2 C_2}{\partial x^2} = \frac{C_2[(x+1,t)] - 2C_2[x,t] + C_2[(x-1,t)]}{\Delta x^2} \quad (11)$$

$$\frac{\partial C_2}{\partial t} = \frac{C_2[x,(t+\Delta t)] - C_2[x,t]}{\Delta t} \quad (12)$$

Substituting Eqs. 9, 10, and 11 in Eq. 7 and Eqs. 9, 11, and 12 in Eq. 8, the change in concentration with respect to time for a particular grid point is obtained as

$$C_1[x,(t+\Delta t)] = C_1[x,t] + A + B \quad (13)$$

$$C_2[x,(t+\Delta t)] = C_2[x,t] + C + D \quad (14)$$

where

$$A = \frac{D_{11}\Delta t}{\Delta x^2}\{C_1[(x+1),t] - 2C_1[x,t] + C_1[(x-1),t]\} \quad (14a)$$

$$B = \frac{D_{12}\Delta t}{\Delta x^2}\{C_2[(x+1),t] - 2C_2[x,t] + C_2[(x-1),t]\} \quad (14b)$$

$$C = \frac{D_{21}\Delta t}{\Delta x^2}\{C_1[(x+1),t] - 2C_1[x,t] + C_1[(x-1),t]\} \quad (14c)$$

$$D = \frac{D_{22}\Delta t}{\Delta x^2}\{C_2[(x+1),t] - 2C_2[x,t] + C_2[(x-1),t]\} \quad (14d)$$

To calculate the change in the values of C_1 and C_2 for each mesh element as a function of Δt from Eqs. 13 and 14, the values of D_{11}, D_{12}, D_{21}, and D_{22} should be known. These values can be calculated as follows.

According to Birchenall and Mehl [25] flux of any diffusing element can be expressed in terms of its activity as

$$J = -D_a\frac{da_C}{dx} \quad (15)$$

where D_a is the activity diffusion coefficient of carbon. If it is assumed that component 1 (carbon) is a relatively dilute interstitial and component 2 (chromium in this case) is a dilute substitutional component of a ternary alloy, then

$$\frac{D_{12}}{D_{11}} \cong \varepsilon_{12}X_1 \quad (16)$$

where X_1 is the mole fraction of component 1. In terms of activity coefficient γ_1, the Wagner interaction parameter is given as

$$\varepsilon_{12} = \left.\frac{\partial(\ln\gamma_1)}{\partial X_2}\right|_{X_1,X_2=0} \quad (17)$$

In such a case D_a can be assumed to be constant. This assumption has been used earlier by Buchmayr [9] and Kucera et al. [26] for simulating the carbon concentration profiles in dissimilar weldments. For ternary alloys, activity of carbon a_C is given by Eq. 1 [16] where the values of interaction parameter are taken as $\varepsilon_C^C = +1.33$ and $\varepsilon_C^{Cr} = -72$ [22] for Fe–Cr–C system and $\varepsilon_C^{Ni} = +2$ [23] for Ni–Cr–C system. Upon substituting Eq. 1 in Eq. 15, the flux can be rewritten as

$$J = -\left\{\left[D(0)(1+\varepsilon_C^C C_1)\exp(\varepsilon_C^C C_1 + \varepsilon_C^{Cr} C_2)\right]\frac{\partial C_1}{\partial x} + \left[D(0)C_1\varepsilon_C^{Cr}\exp(\varepsilon_C^C C_1 + \varepsilon_C^{Cr} C_2)\right]\frac{\partial C_2}{\partial x}\right\} \quad (18)$$

Comparing the above equation with Fick's first law

$$J = -\left\{[D_{11}]\frac{\partial C_1}{\partial x} + [D_{12}]\frac{\partial C_2}{\partial x}\right\} \quad (19)$$

the values of diffusion coefficients for carbon can be obtained as

$$D_{11} = D_C(1+\varepsilon_C^C C_1)\exp(\varepsilon_C^C C_1 + \varepsilon_C^{Cr} C_2) \quad (20)$$

and

$$D_{12} = D_{11}(\varepsilon_C^{Cr} C_2) \quad (21)$$

Similar analogy can be used to calculate diffusion coefficients for chromium as

$$D_{22} = D_{Cr}(1 + \varepsilon_{Cr}^{Cr} C_2) \exp(\varepsilon_C^{Cr} C_1 + \varepsilon_{Cr}^{Cr} C_2) \quad (22)$$

and

$$D_{21} = D_{22}(\varepsilon_C^{Cr} C_1) \quad (23)$$

ε_{Cr}^{Cr} is the Cr–Cr interaction parameter, which is taken as -5 [22]. D_C and D_{Cr} are concentration independent diffusion coefficients, $D(0)$, for carbon and chromium, respectively. In the calculation, values of D_C and D_{Cr} are taken as 1.05×10^{-11} m^2/s and 2.51×10^{-17} m^2/s, respectively, in ferritic steel and as 1.465×10^{-14} m^2/s and 1.48×10^{-19} m^2/s, respectively, in Ni-based interlayer [21].

The above-calculated values for diffusion coefficients are substituted in Eqs. 14a–14d. Knowing the values of C_1 and C_2 for the mesh points x, $x + 1$, and $x - 1$ for a particular time 't,' C (x, $t + \Delta t$) can be calculated. The calculations were carried out on a one-dimensional finite difference mesh with 100 mesh points. To minimize the error, the width of each mesh point Δx is kept as 0.003 mm. Time increment is calculated from the criteria

$$\Delta t \leq \frac{\Delta x^2}{2D} \quad (24)$$

Detailed flow chart of the computer program that was developed to solve the numerical equations is given in Fig. 1.

References

1. Kim BC, Ann HS, Song JT (1992) In: Proceedings of the international trends in welding science and technology. ASM International, Materials Park, Ohio, pp 307–312
2. Albert SK, Gill TPS, Tyagi AK, Mannan SL, Kulkarni SD, Rodriguez P (1997) Weld J 76:135
3. Lundin CD, Khan KK, Yang D (1996) Report No. 1 WRC Bull 407:1
4. Lundin CD, Khan KK, Yang D (1990) In: Proceedings of the recent trends in welding science and technology. ASM International, Materials Park, Ohio, pp 291–297
5. Goldstein JI, Moren AE (1978) Metall Trans 9A:1515
6. Farkas D, Ohla K (1983) Oxid Met 19:99
7. Bongartz K, Lupton DF, Schuster H (1980) Metall Trans 11A:1883
8. Morral JE, Dupen BM, Law CC (1992) Metall Trans 23A:2069
9. Buchmayr B (1990) Fundamentals and applications of ternary diffusion. Pergamon Press, New York, pp 227–240
10. Kirkaldy JS (1971) Oxidation of metals and alloys. ASM, Ohio, pp 101–114
11. Engström A, Höglund L, Ågren J (1994) Metall Trans 25A:1127
12. Kozeschnik E, Pölt P, Brett S, Buchmayr B (2002) Sci Technol Weld Join 7:63
13. Kozeschnik E, Warbichler P, Letofsky-Papst I, Brett S, Buchmayr B (2002) Sci Technol Weld Join 7:69
14. Kucera J, Vrestal J, Stránskỳ K (1989) Defect Diffus Forum 66–69:1395
15. Gauzzi F, Missori S (1988) J Mater Sci 23:782. doi:10.1007/BF01153967
16. Sudha C, Terrance ALE, Albert SK, Vijayalakshmi M (2002) J Nucl Mater 302:193
17. Sudha C, Terrance ALE, Vijayalakshmi M (2002) In: Proceedings of the IIW Asian pacific international congress, Singapore. Welding Institute of Australia, pp 1–15
18. Sudha C, Thomas Paul V, Terrance ALE, Saroja S, Vijayalakshmi M (2006) Weld J 85:71
19. Huang ML, Wang L (1998) Metall Trans 29A:3037
20. Pavlovsky J, Million B, Ciha K, Stránskỳ K (1991) Mater Sci Eng A 149:105
21. Londolt B (1990) Diffusion in solids, metals and alloys. Springer-Verlag, Berlin, pp 372–435
22. Wada H (1985) Metall Trans 16A:1479
23. Lupis CHP (1983) Chemical thermodynamics. Oxford University Press, North Holland, pp 491–501
24. Crank J (1956) The mathematics of diffusion. Oxford University Press, Oxford, pp 150–186
25. Birchenall CE, Mehl RF (1947) Trans AIME 171:143
26. Kucera J, Stránskỳ K (1982) Mater Sci Eng 52:1